Direct synthesis of nanosized CHA zeolite free of organic template by a combination of cations as structure directing agents

Maxime Debost, Edwin B. Clatworthy, Julien Grand, Nicolas Barrier, Nikolai Nesterenko, Jean-Pierre Gilson, Philippe Boullay, Svetlana Mintova

Direct synthesis of nanosized CHA zeolite free of organic template by a combination of cations as structure directing agents

Maxime Debost, [a,b] Edwin B. Clatworthy,[a] Julien Grand [a,c], Nicolas Barrier[b], Nikolai Nesterenko[c], Jean-Pierre Gilson,[a] Philippe Boullay,[b] and Svetlana Mintova*[a]

[a] Normandie Université, ENSICAEN, CNRS, LCS, 14050 Caen, France

[b] Normandie Université, ENSICAEN, CNRS, CRISMAT, 14050 Caen, France

[c] TotalEnergies OneTech Belgium, Feluy, B-7181 Seneffe, Belgium

DEDICATION

We dedicate this article to our dear friend and great scientist Avelino who inspired us along the years and had an enormous positive role in the International Zeolite Community. Avelino has been the model for us and the main resource for ideas, creation of scientific problems and finding the solutions! Thank you for stimulating this work dealing with the synthesis of highly desired CHA-type zeolite nanocrystals for CO_2 adsorption and other related applications. You have been the pioneer in the field!

ABSTRACT

There is an increasing demand for porous materials able to separate the components of natural gas, mainly CH_4 and CO_2. Flexible small pore zeolites are interesting candidates due to their high sorption capacity and ability to selectively separate molecules of similar sizes. This

selectivity comes from their small pores, large cavities, and shapes which can be controlled by the introduction of different extra-framework cations such as Na^+, K^+, Cs^+. Furthermore, the extra-framework cations selectively provide access to the pores and cages of the zeolite depending on the nature of the molecules present. The strategy to prepare CHA-type zeolites across a range of particle sizes, from micron-sized dimensions to nanocrystals with a size of 50 nm, was investigated. The quantities of extra-framework cations and the hydrothermal conditions were optimized in order to avoid the formation of secondary structural phases and selectively target the CHA phase. The CHA-type zeolites were characterized by electron microscopy, MAS NMR and FTIR spectroscopy, and PXRD. The Si/Al ratio of the obtained CHA zeolite was between 1.7 and 2.6 which is ideal for gas separation applications. The nanosized as-synthesised CHA zeolite (Si/Al = 2.4) demonstrates a high CO_2 storage capacity (4.6 mmol/g) making it an ideal candidate for gas separation applications.

KEYWORDS

Zeolites, nanomaterials, cations, adsorption, carbon dioxide

1. INTRODUCTION

Microporous molecular sieves with small pores, *i.e.*, aluminosilicates (zeolites) and silicoaluminophosphates (SAPOs), can be used to separate polar and non-polar molecules (*e.g.* CO_2, CH_4, N_2).[1, 2] Among these materials, SSZ-13, a pure silica zeolite with the chabazite (CHA) topology, is currently utilized in selective catalytic reduction (SCR) while SAPO-34, also possessing the CHA topology, is currently employed for methanol-to-olefins (MTO) catalysis.[3, 4] The separation ability is higher with the aluminosilicate CHA-type zeolite with a Si/Al ratio lower than 3 due to a phenomenon described as the "trapdoor" effect.[5-7] Shang *et al.* have reported that the selectivity towards CO_2 in low-Si alkali metal cation CHA zeolites are

in the order Cs > Rb > K ~ Na ~ Li at 273 K and 100 kPa.[8] Therefore, molecular sieves with frameworks containing cages that have limiting pore sizes consisting of 8 tetrahedral atoms possess the appropriate shape selectivity for small molecule separation. The small pores of the CHA framework topology (0.38 × 0.38 nm) do not allow large molecules to enter into the cages (0.8 × 0.8 × 1.0 nm) where small molecules can access. Previously, CHA zeolite with Si/Al ≈ 2 and K^+ as extra-framework cations (denoted r2KCHA) has shown great potential for the use of temperature-regulated guest admission of H_2 and CH_4 for gas delivery.[6, 9] In addition the Cs form was investigated for the separation of CO_2/CH_4 gas mixtures and D_2/H_2 isotopes.[10] Furthermore, NH_4-CHA zeolite may be a very interesting nanosized material as a starting material to prepare novel catalysts for the MTO reaction.[11]

The synthesis of CHA zeolite is mainly achieved by using organic structure-directing agents (OSDA) such as TEAOH (tetraethylammonium hydroxide), TMAdaOH (tetramethyladamantylammonium hydroxide), CTAB (hexadecyltrimethyl ammonium hydroxide), choline chloride, BTMB (benzyltrimethylammonium bromide), and Cu^{2+}TEPA (Cu-tetraethylenepentamine).[12-14] The high-temperature treatments (calcination) for the removal of OSDAs from crystalline structures is undesirable because of the additional energy requirements, the gas treatment, and the loss of the expensive OSDA. The use of FAU as a starting material for inter-zeolite conversion to obtain K-CHA has drawbacks such as the long time required for synthesis (4 days at 100 °C) and the need to be in the ammonium form which requires calcination prior to use.[15]

Recently our group has developed a low-cost and green preparation method for nanosized CHA-type zeolite.[16] This was achieved without the use of seeds, fluoride, ball milling, zeolite recrystallisation or OSDAs.[17-19] As a consequence of avoiding the use of OSDAs, our strategy of small-pore zeolite synthesis also sidesteps the requirement of a post-treatment step. In addition, a key aspect of the synthesis is the preparation of crystals with dimensions smaller than 100 nm. Nanosized zeolites have shown superior performance in SCR and MTO reactions

and gas adsorption processes because of their relatively larger external surface areas and more rapid diffusion properties.[17, 20, 21] To realise the potential of our synthesis strategy the synthesis space of the nanosized CHA zeolite was explored. We describe the synthesis of CHA-zeolite with narrow particle size distributions by using colloidal precursor solutions involving the variation of the alkali metal cations, silicon and aluminium content, ageing, and hydrothermal treatment time and temperature. The aim is to propose a synthesis route of nanosized Cs,K,Na-CHA, K-CHA and Cs-CHA, three highly interesting materials for gas adsorption or separation. The as-prepared nanosized CHA zeolite was shown to possess an excellent capacity to absorb CO_2 and the ability to discriminate against less polar molecules such as N_2, *i.e.* the "trapdoor" effect. In order to study the adsorption phenomenon and the selectivity, spectroscopic and physisorption characterization methods were used. The results show that the chemical composition of the small pore CHA-type zeolite and the type of extra framework cations played a major role in the behaviour of CO_2 adsorption.

2. EXPERIMENTAL

2.1 Materials, synthesis of nanosized CHA zeolite, and ion exchange.

The procedure for preparing the template-free nanosized CHA zeolite is described below. The variation of the parameters for the optimisation of the synthesis are listed in Table 1. As-synthesised CHA (Run 13, Table 1) was prepared from a precursor mixture with a molar composition: 6 Na_2O: 1.35 K_2O: 0.15 Cs_2O: 0.6 Al_2O_3: 16 SiO_2: 120 H_2O. Double distilled (ddH_2O) from an Aquatron Water Still A4000D was used. $NaAlO_2$ (0.384 g, 47% Na_2O, 53% Al_2O_3, Sigma Aldrich) as aluminium source was dissolved in ddH_2O (2.3 g). NaOH 1.41 g, 97%, Sigma Aldrich) and KOH (0.593 g, 85%, Sigma Aldrich) and CsOH (0.27 g, 50 wt% Cs in H_2O) were added to the aluminium to form a clear solution. The Ludox-AS40 (8.0 g, 40 wt% SiO_2, Sigma Aldrich) was added dropwise to hydroxide solution under vigorous stirring. The resulting suspension was aged at room temperature for 12 days under stirring conditions. During this period, the white suspension turned clear after 3 h of stirring. Then, the hydrothermal

treatment was performed at 90 °C for 8 h. The crystalline product was diluted with 80 °C double distilled water, purified by centrifugation (20000 rpm, 20 min) and finally dispersed in ddH_2O. The resulted suspension was dried at 60 °C for further characterization and the rest was kept as suspension for post-synthetic modifications. Nanosized CHA (Si/Al = 2) was prepared in a similar fashion using the molar oxide ratio described previously.[16]

To investigate the effect of different cations on the CO_2 adsorption, the optimised as-synthesised CHA (Run 13) was ion-exchanged with 0.1 M solutions of alkali metal nitrates (Na^+, K^+, Cs^+), the samples denoted as Na-CHA, K-CHA and Cs-CHA. The zeolite sample (0.2 g) was mixed with the solution (25 mL). This mixture was stirred overnight at room temperature. Afterwards the solution was filtered and washed with ddH_2O, and the zeolite powder was separated. This process is repeated three times. Finally, the samples were dried overnight in an oven at 50 °C prior to calcination. The chemical composition of the samples was determined by inductively coupled plasma mass spectroscopy (ICP).

Micron-sized K-CHA was synthesised following the procedure described by Shang *et al*.[5] Zeolite Y powder (CBV400, 25 g) was mixed with ddH_2O (198 mL) and a solution of KOH (9.5 M, 27 mL) in a sealed 250 mL polypropylene bottle. The mixture was placed in an oven preheated at 95 °C for 15 days. Then the sample was cooled to room temperature and washed with ddH_2O by centrifugation at 20,000 rpm until the supernatant had a pH value between 7 and 8. The washed sample was dried in an oven at 60 °C overnight.

2.2 Characterisation

Powder X-ray Diffraction: Powder X-ray diffraction (PXRD) patterns were collected with a PANalytical X'Pert Pro diffractometer using Cu-$K\alpha_1$ radiation (λ = 1.5406 Å, 45 kV, 40 mA). The unit cell parameters of the samples were obtained from powder diffraction data from Le Bail profile refinement using the JANA2006 software.[22]

Electron Microscopy: Scanning Electron Microscopy (SEM) micrographs were recorded with TESCAN Mira field-emission scanning electron microscope operating at 30 kV. Samples were mounted on a specimen holder using double sided carbon tape and coated with platinum using CRESSINGTON 108 auto evaporative coating machine. Transmission Electron Microscopy (TEM) was used to obtain information on the crystal size, morphology and crystallinity of the materials. In this work high resolution images were obtained using a JEM ARM200F cold FEG double aberration-corrected microscope operated at 200 kV. For TEM observations, fine particles of the as-prepared samples were deposited from suspension and dried on carbon-film covered copper grids.

Solid-State MAS NMR: NMR spectra were recorded on a Bruker Avance III-HD 500 (11.7 T) spectrometer using 4 mm-OD zirconia rotors. Single pulse excitation (30° flip angle) of 3 μs was used for ^{29}Si MAS NMR experiment and 30 s of recycle delay. A spinning frequency of 12 kHz was used for Si. ^{27}Al MAS NMR was done with a p/12 pulse (selective pulse), a spinning speed of 14 kHz and a recycle delay of 1 s.

Elemental Analysis: The elemental analysis of all samples was performed by inductively coupled plasma–atomic emission spectroscopy using an OPTIMA 4300 DV (Perkin–Elmer) instrument.

N_2/CO_2 Surface Area Analysis: N_2 adsorption/desorption and CO_2 adsorption isotherms were measured using a Micrometrics ASAP 2020 volumetric adsorption analyser. Samples were degassed at 350 °C under vacuum overnight prior to the measurement.

Thermogravimetric Analysis (TGA): TGA was carried out on a SETSYS 1750 CS evolution instrument (SETARAM). The sample was heated from 25 °C to 800 °C with a heating ramp of 5 °C.min^{-1} under air (flow rate: 40 mL.min^{-1}).

Fourier-Transformed Infrared Spectroscopy (FTIR): The IR spectra of zeolite samples were recorded using a Nicolet Impact 410 FTIR spectrometer equipped with a MCT detector across

the range of 400–4000 cm^{-1}. The CO_2 adsorption on 20 mg self-supported pellets as-prepared CHA was followed using *in situ* FTIR spectroscopy. The cell was connected to a 10^{-5} Pa high-vacuum. The sample was activated at 350 °C for 2 h to remove the adsorbed water. After cooling to room temperature, a spectrum of the samples before adsorption was recorded for reference. The IR spectra of CO_2 was collected at room temperature; the gas injection was done in small doses.

3. RESULTS AND DISCUSSION

The CHA-type zeolite was prepared in the absence of organic template using inorganic reagents only. The initial synthesis of CHA zeolite had a final precursor suspension with the following molar composition: 8.0 Na_2O / 1.25 K_2O / 0.3 Cs_2O / 10 SiO_2 / 0.8 Al_2O_3 / 120 H_2O. The resulting gel was stirred overnight and treated at 90 °C for 8 h. Elemental analysis of the final CHA sample indicated that the Si/Al ratio is 1.7. SEM images of the CHA sample shows aggregates with a size of 500 nm composed of individual crystallites of 30–150 nm (Figure S1a). The crystallite size was determined by analysis of the powder X-ray diffraction data using the Scherrer equation (Figure S1b).[23] The ^{29}Si MAS NMR spectrum contains peaks at -89.2 ppm, -93.6 ppm, -99.0 ppm, -104.4 ppm and -109.0 ppm corresponding to Q^0 (4Al), Q^1 (3Al), Q^2 (2Al), Q^3 (1Al) and Q^4 (0Al) species, respectively (Figure S1c). A Si/Al ratio of 1.7 was calculated from the ^{29}Si NMR spectra with the equation of Engelhardt and Michel. The obtained CHA possesses interparticle mesoporosity highlighted by the hysteresis loop at higher partial pressure during N_2 adsorption analysis (Figure S1d). The CHA material exhibits a surface area of 64.4 m^2/g and a total pore volume of 0.088 cm^3/g due to the presence of a high number of extra-framework cations.

3.1 Effect of synthesis temperature

The optimization of the synthesis conditions was investigated to obtain discrete CHA crystals in order to improve their diffusion properties for gas adsorption.[21] First, the effect of the synthesis temperature was investigated. CHA zeolite was prepared under hydrothermal conditions within the temperature range of 70–140°C (Figure S2). Pure CHA phase is obtained at synthesis temperatures higher than 90 °C. At lower temperature the formation of BPH is favoured, while higher temperature leads to the formation of the dense phase ANA as shown in Scheme 1.[24] The synthesis time was significantly decreased when increasing the synthesis temperature in order to avoid the formation of ANA (Table S1.). The Si/Al ratio (1.7–1.8) of the obtained crystals was independent of the synthesis temperature; synthesis above 140 °C resulted in the formation of agglomerates and crystals with larger sizes. The CHA zeolite obtained at different temperatures consists of spherical aggregates with a temperature dependent particle size of 500–5000 nm (Table S1).

3.2 Effect of the initial composition of the precursor suspensions

The synthesis parameters explored for optimising the composition of the precursor suspension to obtain discrete, non-aggregated, nanosized CHA are summarised in Table 1. The synthesis results employing hydrothermal treatment for 8 h at 90 °C demonstrate the importance of the three alkali-metal hydroxides to obtain the nanosized CHA phase (Run 1). By excluding sodium, an amorphous material is obtained (Run 2). The high concentration of Na^+ cations is necessary to help solubilise silica, stabilise the colloidal suspension, and promote the formation of nucleates. The absence of K^+ leads to the formation of RHO (Run 3), corresponding to the procedure described by Grand *et al*.[25] The absence of Cs^+ results in the formation of FAU (Run 4), which is similar to the synthesis proposed by Iwama and co-workers.[26] Considering the role of alkali metal cations on the formation of CHA and RHO under the hydrothermal conditions employed in this work, we may propose that the formation of zeolite topologies with eight-membered rings (8MRs) is favoured in the presence of Cs^+ cations.[27] Iwama and co-workers proposed that K^+ and Na^+ cations favour the formation of 6MR and 4MR structures

respectively. The mixture of the three cations and their relative amounts are critical factors for controlling the CHA zeolite crystallization.[26]

The phase diagram representing the crystallization field of the nanosized CHA zeolite in the presence of different amounts of K_2O (y-axis) and Cs_2O (x-axis) is presented in Figure S3. Again, the synthesis time is adapted to avoid the formation of ANA: the synthesis of some zeolites is more rapid than others. For example, the RHO (y = 0 and x = 0.6) requires 75 min of hydrothermal treatment at 90 °C, while CHA (y = 1.0 and x = 0.4) begins to be crystallise after 8 h. Crystalline CHA-type zeolite was obtained in a short crystallization range between x = 0.3–0.6 and y = 0.6–1.25. The precursor suspensions with the K_2O:Cs_2O ratios of 0.3:1.25, 0.4:1.0 and 0.6:0.7 provided pure CHA. Reducing the Cs_2O or the K_2O amount results in impurities such as BPH and RHO. Likewise, increasing the overall hydroxide content leads to the formation of EDI (Run 5). In view of the experimental conditions, it is clear that the less dense phases such as FAU and RHO are formed under low content of KOH and CsOH. SEM images of the phases obtained from precursor suspensions with different alkali metal cations are shown in Figure S4.

It has previously been demonstrated that the agitation action during the synthesis process is a key factor in controlling the dimensions of zeolite particles.[28] Here, the ageing of the precursor suspensions at room temperatures has a significant influence on the crystallization process.[29] First, the stirring time was modified leading to a small decrease of the aggregate size. Unfortunately, the formation of Linde Q (BPH-type aluminosilicates) as a side product (Run 6) increased with the stirring time. After 12 days of stirring, despite performing the hydrothermal treatment at 90 °C, BPH phase was obtained (Run 7) without the presence of CHA phase. The preparation of BPH nanosheets has recently been investigated by Clatworthy *et al*.[30] To prevent the formation of BPH and reduce the crystal size, the NaOH content was reduced (Runs 8-13) and the Si/Al ratio was increased (Runs 10-13). This strategy allows synthesizing individual non-aggregated crystals; the Cs^+ cation content was reduced to

completely avoid the formation of ANA while the K^+ content was increased slightly to maintain the hydroxide concentration (Runs 12 and 13). Finally, individual CHA crystals were obtained (Run 13) by increasing the stirring time and adjusting the chemical composition of the precursor suspensions. The SEM images are shown in Figure S5. The sample from Run 13, denoted as-synthesised CHA, fulfils all the pre-defined criteria: the sample is composed of nanosized individual non-aggregated particles and possesses a Si/Al ratio of 2.4.

LeBail refinement based on the PXRD pattern of the as-synthesised CHA is shown in Figure 1. No impurity phases were detected in the sample; the pattern exhibits Bragg peaks expected for pure CHA zeolite. The pattern displays anisotropic peak broadening due to the plate-like shape of the crystallites with a thickness of 15 nm and a length of 80 nm (*R*-3*m* space group) determined by the Scherrer equation.[23] TEM analysis reveals that the particles are well dispersed (Figure S5f). HR-TEM images reveal uniform nanosized crystals with a size of 15–100 nm and a plate-like morphology (Figure 1a).

Further structural information is provided by ^{29}Si MAS NMR spectroscopy (Figure 1c). The spectrum of the hydrated as-synthesised CHA sample allowed for the determination of the Si/Al ratio as 2.4. From the ^{27}Al MAS NMR analysis a single peak corresponding to aluminium in a tetrahedral position can be observed at around 58.0 ppm; no peak corresponding to octahedral aluminium was observed at 0 ppm (Figure S6).

The N_2 adsorption and desorption isotherms of the as-synthesised CHA are shown in Figure 1d. The nanozeolite exhibits a type IV isotherm due to the negligible uptake of N_2 low partial pressure (P/P_0). This indicates that N_2 does not have access to the internal surface of the zeolite because of cations such as Cs^+ or K^+ occupying the 8MRs, as is the case for zeolites displaying "trapdoor" behaviour.[7] The sample shows a large H1-type hysteresis at high partial pressure, attributed to the textural pores formed by the close packing of mono-dispersed nanosized crystallites. The measurement demonstrated that the nanocrystals are fully dispersed with an external surface of 70.4 m^2/g.

The amount of water in the as-synthesised CHA was determined by thermogravimetric (TG) analysis. The sample showed a 13% loss of weight attributed to water upon heating to 250 °C (Figure S7). The TG measurement highlights the absence of OSDA to synthesise the CHA structure.

3.3 Ion exchange of as-synthesised CHA

The nanosized as-synthesised CHA zeolite sample was ion-exchanged with $Cs(NO_3)$, $K(NO_3)$ and $Na(NO_3)$. PXRD patterns of the three ion-exchanged samples corresponds to the typical pattern described in the literature (Figure 2).[31, 32] The form of the Na-CHA is well preserved after ion exchange treatment whereas the structure typically collapses after calcination when the Si/Al is lower than 2.0. The porosity of the zeolite nanoparticles determined by N_2 sorption analysis before and after ion-exchange treatment are presented in Figure 3 and Table S2. The as-synthesised CHA, K-CHA and Cs-CHA exhibit a Type II, indicating that the micropores are not accessible, but high adsorption uptake at high P/P_0 demonstrates the high textural mesoporosity of packed zeolite nanoparticles. In contrast, Na-CHA shows a Type I isotherm characteristic for microporous materials. The K^+ and Cs^+ cations, when located in the 8MRs, restrict the access of N_2 to the cages while the Na^+ cations occupy positions inside the cages.[7, 33-35]

3.4 Adsorption of CO_2 on as-synthesised and ion-exchanged CHA

The CO_2 adsorption isotherms of the as-synthesised and ion-exchanged CHA measured at 0 °C are presented in Figure 4. The adsorption capacities of the as-synthesised CHA and Na-CHA have similar values (4.6 and 4.1 mmol/g respectively at 121 kPa). In contrast, Cs-CHA sample has the lowest CO_2 adsorption capacity consistent with other Cs-CHA samples reported in the literature (2.2 mmol/g at 121 kPa, 0 °C). The lower CO_2 adsorption capacity is attributed to the size and the polarity of the Cs extra-framework cations. The CO_2 uptake increases less steeply at low pressures of CO_2 on Cs-CHA. The as-synthesised CHA is also compared to the micron-sized K-CHA (Si/Al = 2) prepared from the patent literature, and nanosized CHA (Si/Al = 2)

that we reported previously.[5, 15, 16] It is worth noting that the Na-CHA, K-CHA, Cs-CHA and micron-sized K-CHA display similar adsorption isotherm shapes, different from the tri-cationic samples. All samples exhibited a rapid uptake of CO_2 at low absolute pressure (< 40 kPa) followed by a relatively flat step at high absolute pressure (> 40 kPa). Slight differences can be observed over tri-cationic samples (Figure 4) regarding the second adsorption stage: it is possible to distinguish a continued increase of CO_2 adsorption.

3.5 In situ IR adsorption of CO_2 on as-synthesised and ion-exchanged CHA

In situ IR spectroscopy was carried out to study the CO_2 sorption behaviour of the as-synthesised and ion-exchanged CHA samples. Figure S8 presents the FTIR spectra of CO_2 adsorbed on the as-synthesised CHA. The dehydration of the sample was successfully performed evidenced by the absence of the band at 1627 cm^{-1} corresponding to adsorbed water. Here, three different regions evolved with the increase of the CO_2 partial pressure: A) 1800–1200 cm^{-1}, B) 2400–2300 cm^{-1} and C) 3400–3800 cm^{-1}. Regions (B) and (C) are characteristic of physisorbed CO_2 while region (A) is characteristic of chemisorbed CO_2 (carbonate) species. A well pronounced adsorption band at 2347 cm^{-1} is observed corresponding to the asymmetric stretching mode of physically adsorbed carbon dioxide on the zeolite surface, as well as a characteristic band at 3703 cm^{-1} corresponding to a combination of vibration modes. In addition, the bridged bidentate carbonate formation is indicated by the bands at 1350 and 1324 cm^{-1}. The observed peaks are in accordance with observations on low silica FAU and LTA type zeolites studied with this method.[36, 37]

Figure S8b shows that the chemisorption bands change negligibly between low pressure (P/P_0 < 0.01 bar) and moderate pressures indicative of a low number of chemisorption sites, consistent with previous work.[32] On the other hand, the characteristic bands of the physisorbed CO_2 continue to increase in intensity (band at 3703 cm^{-1}) and in thickness (band at 2347 cm^{-1}). Then, the CO_2 desorption procedure was recorded at room temperature on the as-synthesised CHA. The characteristic bands of physisorbed CO_2 decrease simultaneously with the reduction in

pressure. In contrast, the bands corresponding to carbonate species do not change with the decrease of pressure. A temperature elevation to 250 °C was required to significantly desorb the carbonates.

The as-synthesised and ion-exchanged CHA samples show different behaviour in the adsorbing and desorbing of CO_2. The CO_2 adsorption capacity is different for each ion-exchanged nanosized CHA, consistent with the isotherm measurements. The interaction between the CO_2 with the zeolite framework and extra-framework cations explains those differences. Figure S9 shows the FTIR spectra collected during adsorption of CO_2 on the ion-exchanged CHA zeolites. The samples exhibited carbonate bands similar to the as-synthesised CHA. Figure S9b shows that the Cs-CHA has a high relative intensity of chemisorbed CO_2 to physisorbed CO_2 due to the overall lower amount of physisorbed CO_2 on this sample. In comparison, K-CHA, Na-CHA and as-synthesised CHA have more intense bands of carbonate species; the integration of these bands suggests that Cs-CHA forms fewer carbonate species compared to the other samples (Figure 5). Interestingly, the physisorbed υ_3 vibrational mode for the as-synthesised CHA and K-CHA is observed at the same wave number, but for Cs-CHA and Na-CHA it appears at a frequency other than 2347 cm^{-1}. The υ3 frequency appears at 2343 cm^{-1}, and 2345–2362 cm^{-1} for Cs-CHA and Na-CHA respectively. The relatively small shifts are the consequence of the M^+–O=C=O interaction (Figure S9).

The FTIR spectra of the Na-CHA sample with an increasing amount of adsorbed CO_2 are presented in Figure S9c. The amount of physisorbed CO_2 on the Na-CHA sample is higher than on the other CHA samples. The bands around the 2300 cm^{-1} band is composed of 3 different bands at 2345 cm^{-1} (area: 56 %, FWHH: 4.19 cm^{-1}), 2355.5 cm^{-1} (38%, 6.77 cm^{-1}) and 2363.6 cm^{-1} (6 %, 5.41 cm^{-1}). The significant difference in the structure of the band of the physisorbed CO_2 around 2300 cm^{-1} for the Na-CHA compared to the K-CHA and Cs-CHA may be due to the difference in the location of the Na^+ extra-framework cations and as a consequence the CO_2 adsorption modes. K^+ and Cs^+ extra-framework cations are known to preferentially occupy the

8MRs of the CHA cage which can facilitate high adsorption selectivity towards CO_2 over nonpolar molecules such as N_2 and CH_4 due to "trapdoor" behaviour.[5] This temperature-dependent phenomenon is due to the ability of CO_2 to interact more strongly with the cations occupying the 8MRs facilitating selective entry to the mircopore network, while relatively weakly interacting molecules, such as N_2 and CH_4, cannot gain access. We have previously reported for mixed-cation $Cs^+/K^+/Na^+$ nanosized CHA (Si/Al = 2) loaded with CO_2 that the molecules are arranged near-parallel to the long axis within the CHA cage.[16] Contrary to the K-CHA and Cs-CHA which exhibit "trapdoor" behaviour, the supercage of Na-CHA is accessible to small non-polar molecules due to the low occupation of Na^+ in the 8MRs.[38] As a consequence, some CO_2 molecules might be sited in the 8-membered ring as has been reported for higher Si-containing CHA zeolites such as SSZ-13 with Si/Al ratios of 6 and 12.[39] This behaviour was also observed on medium and large pore zeolites.[37, 40]

Overall, this study has identified the adsorption performance at different pressures of CO_2. The isotherm of the mixed-cation as-synthesised CHA showed more adsorbed CO_2 at a partial pressure up to 40 kPa than the mono-cationic K-CHA and Cs-CHA. Curiously, the ion exchange procedure changed the curve profile, thereby excluding the hypothesis that the crystallite size is the cause of this trend modification (Figure S10). The difference might come from the absorption mode: the FTIR measurements demonstrated the as-synthesised CHA possessed the highest adsorption of chemisorbed CO_2 compared to the mono-cationic variants. For Na-CHA, the Na^+ extra-framework cations favour the adsorption of CO_2 in a chemisorbed manner, yet due to their smaller size also allow for a greater amount of CO_2 to be physisorbed. In comparison, for Cs-CHA the high amount of Cs^+ extra-framework cations significantly reduces the amount of physisorbed CO_2, as well as the amount of chemisorbed CO_2. The K-CHA exhibits a significant amount of physisorbed CO_2 but also less chemisorbed CO_2, similar to the Cs-CHA.

4 CONCLUSIONS

Nanosized CHA-type small-pore zeolites were synthesized in the absence of OSDAs. By proper control of the gel composition and the hydrothermal treatment, the CHA-type zeolite was obtained while avoiding the formation of secondary phases such as EDI, ANA, BPH and RHO. Across the synthesis conditions explored the CHA zeolite samples are either monodispersed or form aggregates with a size between 400 nm and 2000 nm. The synthesis strategy to prepare phase-pure, monodispersed and discrete particles was developed. Monodispersed and nanosized CHA zeolite samples with a Si/Al ratio of 2.4 and an average crystal size of 80–250 nm were obtained. The properties of the nanosized CHA zeolite samples were determined by a combination of spectroscopic, physical and chemical analyses (^{29}Si and ^{27}Al MAS NMR, ICP, PXRD and N_2 sorption).

Ion-exchange of the optimised nanosized CHA was accomplished and their performance for CO_2 adsorption was explored by isotherm analysis and *in situ* FTIR analysis in the presence of CO_2. The CO_2 adsorption isotherms of the parent and ion exchanged samples exhibited comparable CO_2 adsorption capacity to the related materials already reported in the literature, however, the as-prepared tri-cationic nanosized CHA exhibits a less steep slope of the CO_2 isotherm and an overall higher adsorption capacity compared to the samples exchanged with a single cation. With the appropriate ion exchange this material has significant potential for use in the application of temperature-regulated guest admission mechanism of small molecules, isotope separation, and catalytic applications.

ACKNOWLEDGEMENTS

Financial support from the Centre for zeolites and nanoporous materials, Label of Excellence, Normandy Region (CLEAR) is acknowledged. Industrial Chair ANR-TOTAL “Nanoclean Energy” (Grant IPA 5621) is acknowledged, as well as from the Normandy Region through the RIN Recherche Program (Grant 18P01675).

REFERENCES

[1] A. Samanta, A. Zhao, G.K. Shimizu, P. Sarkar, R. Gupta, Post-combustion CO_2 capture using solid sorbents: a review, Ind. Eng. Chem. Res., 51 (2012) 1438-1463.

[2] M. Abu Ghalia, Y. Dahman, Development and evaluation of zeolites and metal–organic frameworks for carbon dioxide separation and capture, Energy Technol., 5 (2017) 356-372.

[3] F. Gao, J.H. Kwak, J. Szanyi, C.H. Peden, Current understanding of Cu-exchanged chabazite molecular sieves for use as commercial diesel engine DeNOx catalysts, Top. Catal., 56 (2013) 1441-1459.

[4] Q. Sun, Z. Xie, J. Yu, The state-of-the-art synthetic strategies for SAPO-34 zeolite catalysts in methanol-to-olefin conversion, Natl. Sci. Rev., 5 (2018) 542-558.

[5] J. Shang, G. Li, R. Singh, Q. Gu, K.M. Nairn, T.J. Bastow, N. Medhekar, C.M. Doherty, A.J. Hill, J.Z. Liu, P.A. Webley, Discriminative separation of gases by a "molecular trapdoor" mechanism in chabazite zeolites, J. Am. Chem. Soc., 134 (2012) 19246-19253.

[6] J. Shang, G. Li, R. Singh, P. Xiao, J.Z. Liu, P.A. Webley, Potassium chabazite: a potential nanocontainer for gas encapsulation, J. Phys. Chem. C, 114 (2010) 22025-22031.

[7] T. De Baerdemaeker, D. De Vos, Gas separation: trapdoors in zeolites, Nat. Chem., 5 (2013) 89.

[8] J. Shang, G. Li, R. Singh, P. Xiao, J.Z. Liu, P.A. Webley, Determination of composition range for "molecular trapdoor" effect in chabazite zeolite, J. Phys. Chem. C, 117 (2013) 12841-12847.

[9] G.K. Li, J. Shang, Q. Gu, R.V. Awati, N. Jensen, A. Grant, X. Zhang, D.S. Sholl, J.Z. Liu, P.A. Webley, Temperature-regulated guest admission and release in microporous materials, Nat. Commun., 8 (2017) 1-9.

[10] A.J. Physick, D.J. Wales, S.H. Owens, J. Shang, P.A. Webley, T.J. Mays, V.P. Ting, Novel low energy hydrogen–deuterium isotope breakthrough separation using a trapdoor zeolite, Chem. Eng. J., 288 (2016) 161-168.

[11] Y. Ji, M.A. Deimund, Y. Bhawe, M.E. Davis, Organic-free synthesis of CHA-type zeolite catalysts for the methanol-to-olefins reaction, ACS Catal., 5 (2015) 4456-4465.

[12] L. Ren, L. Zhu, C. Yang, Y. Chen, Q. Sun, H. Zhang, C. Li, F. Nawaz, X. Meng, F.-S. Xiao, Designed copper–amine complex as an efficient template for one-pot synthesis of Cu-SSZ-13 zeolite with excellent activity for selective catalytic reduction of NO_x by NH_3, Chem. Commun., 47 (2011) 9789-9791.

[13] S.I. Zones, Zeolite SSZ-13 and its method of preparation, Chevron Research Company1985.
[14] L. Xie, F. Liu, L. Ren, X. Shi, F.-S. Xiao, H. He, Excellent performance of one-pot synthesized Cu-SSZ-13 catalyst for the selective catalytic reduction of NO_x with NH_3, Environ. Sci. Technol., 48 (2014) 566-572.
[15] M. Bourgogne, J.-L. Guth, R. Wey, Process for the preparation of synthetic zeolites, and zeolites obtained by said process, Compagnie Francaise de Raffinage1985.
[16] M. Debost, P.B. Klar, N. Barrier, E.B. Clatworthy, J. Grand, F. Lainé, P. Brazda, L. Palatinus, N. Nesterenko, P. Boullay, S. Mintova, Synthesis of discrete CHA zeolite nanocrystals without organic templates for selective CO_2 capture, Angew. Chem. Int. Ed., 59 (2020) 23491-23495.
[17] Z. Li, M.T. Navarro, J. Martínez-Triguero, J. Yu, A. Corma, Synthesis of nano-SSZ-13 and its application in the reaction of methanol to olefins, Catal. Sci. Technol., 6 (2016) 5856-5863.
[18] C. Anand, T. Kaneda, S. Inagaki, S. Okamura, H. Sakurai, K. Sodeyama, T. Matsumoto, Y. Kubota, T. Okubo, T. Wakihara, Downsizing the K-CHA zeolite by a postmilling-recrystallization method for enhanced base-catalytic performance, New J. Chem., 40 (2016) 492-496.
[19] C. Peng, Z. Liu, A. Horimoto, C. Anand, H. Yamada, K. Ohara, S. Sukenaga, M. Ando, H. Shibata, T. Takewaki, Preparation of nanosized SSZ-13 zeolite with enhanced hydrothermal stability by a two-stage synthetic method, Microporous Mesoporous Mater., 255 (2018) 192-199.
[20] M. Chen, Q. Sun, G. Yang, X. Chen, Q. Zhang, Y. Zhang, X. Yang, J. Yu, Enhanced performance for selective catalytic reduction of NO_x with NH_3 over nanosized Cu/SAPO- 34 catalysts, ChemCatChem, 11 (2019) 3865-3870.
[21] X. Tang, J. Liu, H. Shang, L. Wu, J. Yang, Gas diffusion and adsorption capacity enhancement via ultrasonic pretreatment for hydrothermal synthesis of K-KFI zeolite with nano/micro-scale crystals, Microporous Mesoporous Mater., 297 (2020) 110036.
[22] V. Petříček, M. Dušek, L. Palatinus, Crystallographic computing system JANA2006: general features, Z. Kristallogr. - Cryst. Mater., 229 (2014) 345-352.
[23] A. Patterson, The Scherrer formula for X-ray particle size determination, Phys. Rev., 56 (1939) 978.
[24] A. Navrotsky, O. Trofymluk, A.A. Levchenko, Thermochemistry of microporous and mesoporous materials, Chem. Rev., 109 (2009) 3885-3902.

[25] J. Grand, N. Barrier, M. Debost, E.B. Clatworthy, F. Laine, P. Boullay, N. Nesterenko, J.-P. Dath, J.-P. Gilson, S. Mintova, Flexible Template-Free RHO Nanosized Zeolite for Selective CO_2 Adsorption, Chem. Mater., 32 (2020) 5985-5993.
[26] M. Iwama, Y. Suzuki, J. Plévert, K. Itabashi, M. Ogura, T. Okubo, Location of alkali ions and their relevance to crystallization of low silica X zeolite, Cryst. Growth Des., 10 (2010) 3471-3479.
[27] S. Ghojavand, E.B. Clatworthy, A. Vicente, E. Dib, V. Ruaux, M. Debost, J. El Fallah, S. Mintova, The role of mixed alkali metal cations on the formation of nanosized CHA zeolite from colloidal precursor suspension, J. Colloid Interface Sci., 604 (2021) 350-357.
[28] Z. Bohström, B. Arstad, K.P. Lillerud, Preparation of high silica chabazite with controllable particle size, Microporous Mesoporous Mater., 195 (2014) 294-302.
[29] L. Tosheva, V.P. Valtchev, Nanozeolites: synthesis, crystallization mechanism, and applications, Chem. Mater., 17 (2005) 2494-2513.
[30] E.B. Clatworthy, M. Debost, N. Barrier, S.p. Gascoin, P. Boullay, A.l. Vicente, J.-P. Gilson, J.-P. Dath, N. Nesterenko, S. Mintova, Room-Temperature Synthesis of BPH Zeolite Nanosheets Free of Organic Template with Enhanced Stability for Gas Separations, ACS Appl. Nano Mater, 4 (2020) 24-28.
[31] M. Kong, Z. Liu, T. Vogt, Y. Lee, Chabazite structures with Li^+, Na^+, Ag^+, K^+, NH_4^+, Rb^+ and Cs^+ as extra-framework cations, Microporous Mesoporous Mater., 221 (2016) 253-263.
[32] S. Ghojavand, B. Coasne, E.B. Clatworthy, R. Guillet-Nicolas, P. Bazin, M. Desmurs, L. Jacobo Aguilera, V. Ruaux, S. Mintova, Alkali Metal Cations Influence the CO_2 Adsorption Capacity of Nanosized Chabazite: Modeling vs Experiment, ACS Appl. Nano Mater, 5 (2022) 5578-5588.
[33] V.M. Georgieva, E.L. Bruce, M.C. Verbraeken, A.R. Scott, W.J. Casteel Jr, S. Brandani, P.A. Wright, Triggered Gate Opening and Breathing Effects during Selective CO_2 Adsorption by Merlinoite Zeolite, J. Am. Chem. Soc., 141 (2019) 12744-12759.
[34] Z. Bacsik, O. Cheung, P. Vasiliev, N. Hedin, Selective separation of CO_2 and CH_4 for biogas upgrading on zeolite NaKA and SAPO-56, Appl. Energy, 162 (2016) 613-621.
[35] T. Remy, E. Gobechiya, D. Danaci, S. Peter, P. Xiao, L. Van Tendeloo, S. Couck, J. Shang, C. Kirschhock, R. Singh, Biogas upgrading through kinetic separation of carbon dioxide and methane over Rb-and Cs-ZK-5 zeolites, RSC Adv., 4 (2014) 62511-62524.
[36] Q. Liu, A. Mace, Z. Bacsik, J. Sun, A. Laaksonen, N. Hedin, NaKA sorbents with high CO_2-over-N_2 selectivity and high capacity to adsorb CO_2, Chem. Commun., 46 (2010) 4502-4504.

[37] M. Polisi, J. Grand, R. Arletti, N. Barrier, S. Komaty, M. Zaarour, S. Mintova, G. Vezzalini, CO_2 adsorption/desorption in FAU zeolite nanocrystals: in situ synchrotron X-ray powder diffraction and in situ Fourier Transform Infrared spectroscopic study, J. Phys. Chem. C, 123 (2019) 2361-2369.
[38] L.J. Smith, H. Eckert, A.K. Cheetham, Site preferences in the mixed cation zeolite, Li, Na-chabazite: a combined solid-state NMR and neutron diffraction study, J. Am. Chem. Soc., 122 (2000) 1700-1708.
[39] T.D. Pham, M.R. Hudson, C.M. Brown, R.F. Lobo, Molecular basis for the high CO_2 adsorption capacity of chabazite zeolites, ChemSusChem, 7 (2014) 3031-3038.
[40] L. Ohlin, P. Bazin, F. Thibault-Starzyk, J. Hedlund, M. Grahn, Adsorption of CO_2, CH_4, and H_2O in zeolite ZSM-5 studied using in situ ATR-FTIR spectroscopy, J. Phys. Chem. C, 117 (2013) 16972-16982.

TABLES

Table 1. Screening of chemical composition to obtain nanosized dispersed CHA.

Run	**Chemical composition**						**Ageing/ hydrothermal treatment**			**Properties**		
	Na_2O	K_2O	Cs_2O	SiO_2	Al_2O_3	H_2O	Stir. Time (d)	Synth. Time (h)	Synth. Temp. (°C)	Phase*	Si/Al (w/w)	Particle size (nm)
1	8	1.25	0.30	10	0.8	120	1	8	90	CHA	1.7	500
2	-	1.25	0.30	10	0.8	120	1	8	90	Am.	-	-
3	8	-	0.30	10	0.8	120	1	8	90	RHO	1.4	210
4	8	1.25	-	10	0.8	120	1	8	90	FAU	1.4	200
5	8	1.7	0.3	10	0.8	120	1	8	90	EDI	1.2	200
6	8	1.25	0.30	10	0.8	120	4	8	90	CHA (BPH)	1.6	600
7	8	1.25	0.30	10	0.8	120	12	8	90	BPH	1.4	< 100
8	6	1.25	0.30	10	0.8	120	4	8	90	CHA	1.8	1000
9	6	1.25	0.30	10	0.8	120	12	8	90	CHA	1.8	2000

10	6	1.25	0.30	16	0.6	120	12	3	90	CHA/ ANA	2.6	200
11	6	1.25	0.30	16	0.6	120	12	2.5	90	CHA	2.6	200
12	6	1.35	0.15	16	0.6	120	4	8	90	CHA	2.4	300
13	6	1.35	0.15	16	0.6	120	12	8	90	CHA	2.4	< 100

FIGURES

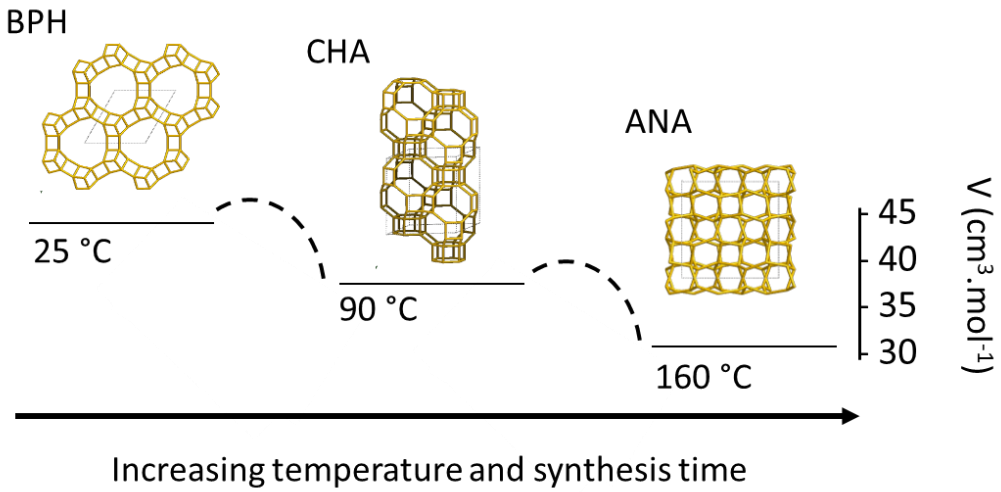

Scheme 1. Stages of the transformation of the zeolite phase with increasing temperature and synthesis time. The relative enthalpy of formation, $\Delta H_f - \Delta H_o$, for zeolite structures is assumed to be proportional to its molar volume, V.

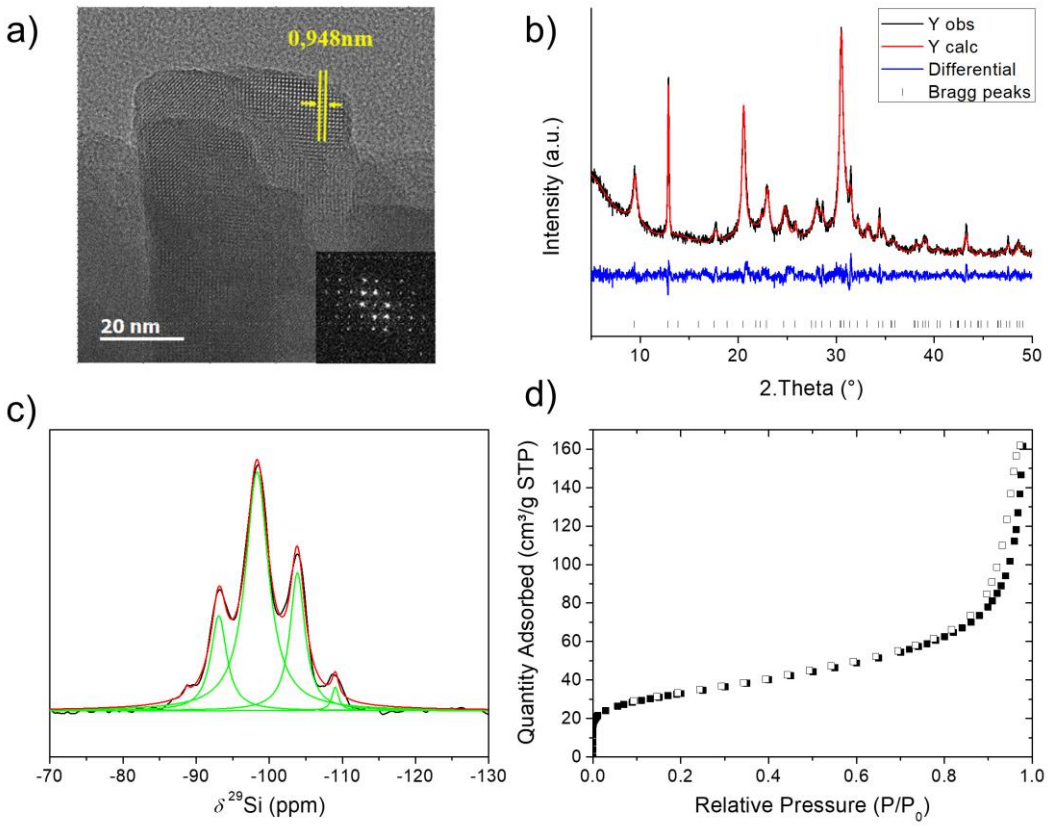

Figure 1. Main physicochemical properties of the as-synthesised CHA (Run 13). (a) HR-TEM of the nanosized CHA and FFT (insert), (b) PXRD pattern of the nanosized CHA. The unit-cell volume and space-group of samples were obtained from X-ray diffraction data based on pseudo-Voigt profile function using the JANA2006 software. Difference plots (blue) and vertical sticks corresponding to Bragg peaks of the CHA phase *R*-3*m* are shown down to the pattern. (c) ^{29}Si MAS NMR spectrum and (d) N_2 adsorption/desorption isotherm recorded at −196 °C.

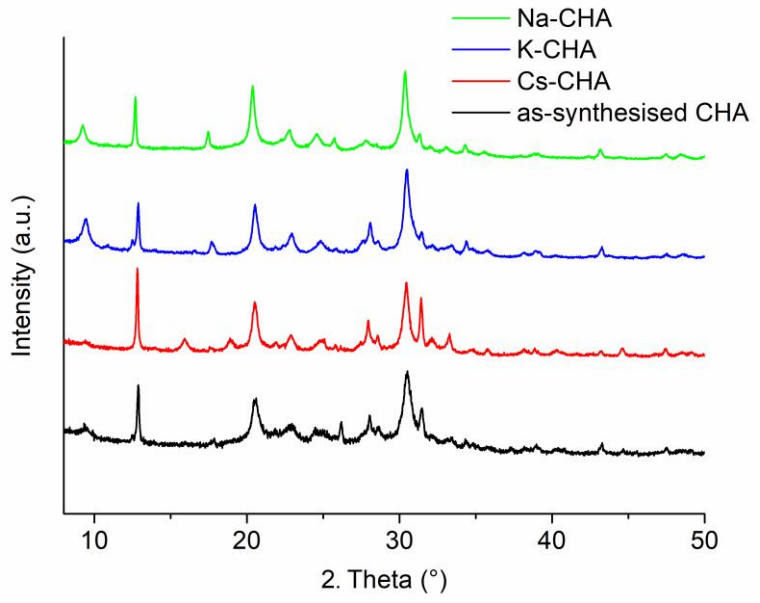

Figure 2. PXRD patterns of the as-synthesised and ion-exchanged CHA zeolite samples.

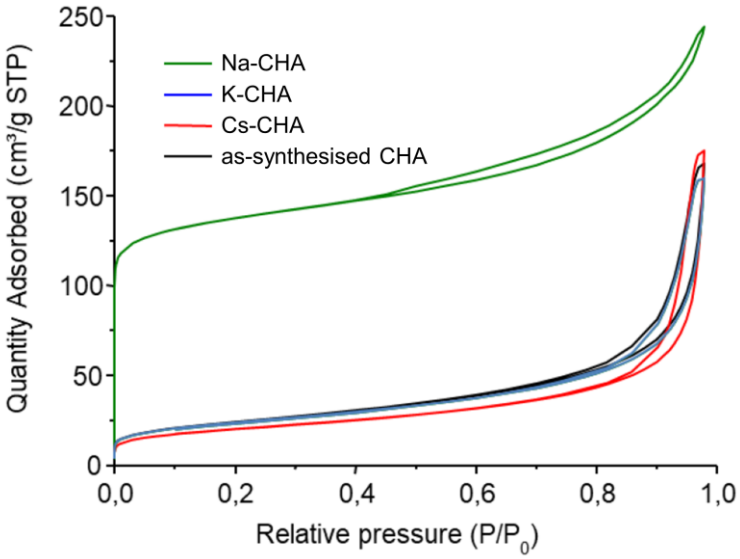

Figure 3. N_2 adsorption and desorption isotherms of the as-synthesised and ion-exchanged CHA zeolite samples.

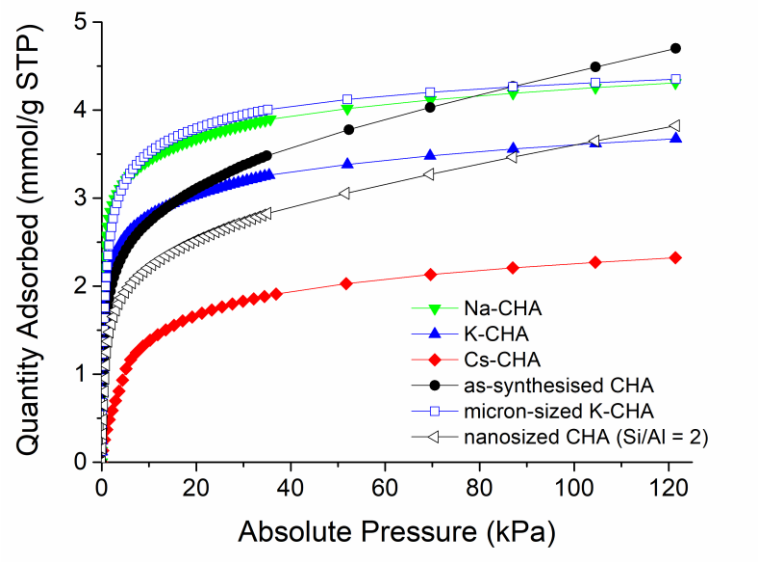

Figure 4. CO_2 adsorption isotherms of as-synthesised and ion-exchanged CHA, micron-sized K-CHA, and nanosized CHA (Si/Al = 2) at 0 °C.

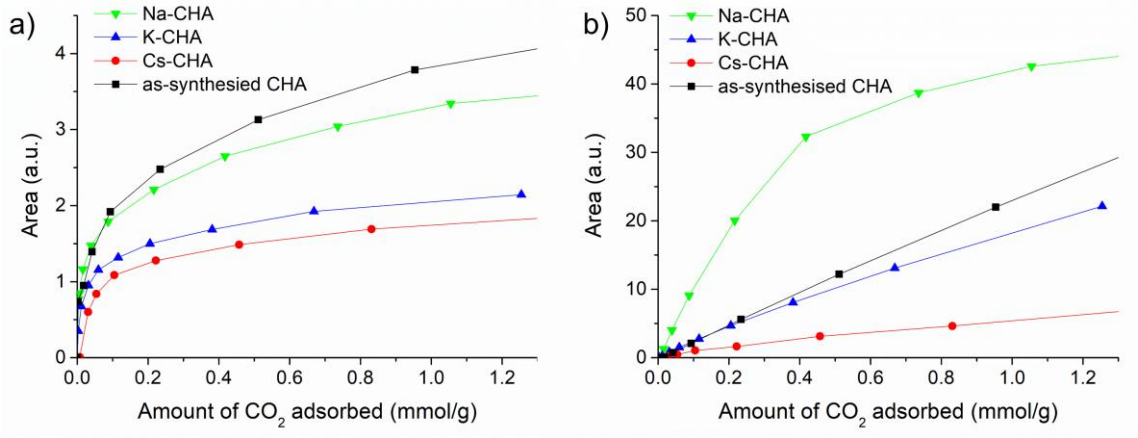

Figure 5. CO_2 species chemisobed (a) and physisorbed (b) followed by FTIR on nanosized CHA samples at 25 °C: Cs-CHA (red), K-CHA (blue), Na-CHA (green) and the as-synthesised sample (black).